Inorganic Chemistry

Article

pubs.acs.org/IC

Establishing the Two-Photon Linkage Isomerization Mechanism in the Nitrosyl Complex *trans*-$[RuCl(NO)(py)_4]^{2+}$ by DFT and TDDFT

Juan Sanz García,[†] Fabienne Alary,[†] Martial Boggio-Pasqua,[†] Isabelle M. Dixon,[†] Isabelle Malfant,[‡] and Jean-Louis Heully*[,†]

[†]Laboratoire de Chimie et Physique Quantiques, UMR 5626, IRSAMC, CNRS et Université de Toulouse, 118 route de Narbonne, 31062 Toulouse, France

[‡]Laboratoire de Chimie de Coordination, CNRS UPR 8241, 205 route de Narbonne, 31077 Toulouse, France

Supporting Information

ABSTRACT: The density functional theory calculations presented in this work allow the first rationalization of the full linkage photoisomerization mechanism of *trans*-$[RuCl(NO)(py)_4]^{2+}$, in both the forward and reverse directions. These mechanisms are consistent with the experimental data establishing that blue-light irradiation triggers the forward process, while red or IR photons trigger the reverse process. Characterization of the singlet and lowest triplet potential energy surfaces shows that, despite the unfavorable thermodynamic character of the forward process, the topologies of the surfaces and particularly some crucial surface crossings enable the isomerization. In the forward Ru−NO → Ru−ON direction, a sequential two-photon absorption mechanism is unraveled that involves a sideways-bonded metastable state. In contrast, in the reverse reaction, two mechanisms are proposed involving either one or two photons.

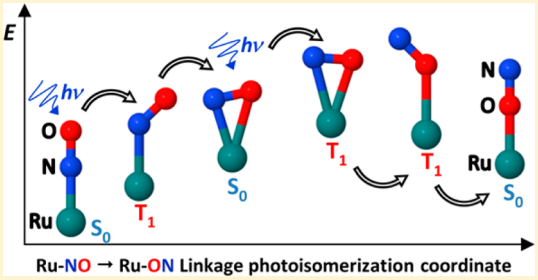

1. INTRODUCTION

Since the discovery of the light-induced metastable isomers of the iron nitrosyl complex $Na_2[Fe(CN)_5(NO)]$ (sodium nitroprusside),[1,2] several iron compounds with similar photophysical properties have been found.[3−10] Because of their photochromic properties, these complexes offer not only a wide range of technological applications such as the design of new optical high-capacity storage devices but also important knowledge in the fundamentals of chemical bonding and photochemical reactions.[11−14] A few years later, photoisomerizable ruthenium nitrosyl compounds have been developed.[15−26] By extension of the nitroprusside terminology, the lowest ground-state species (denoted as **GS**) is characterized by the commonly known N-bound form of the nitrosyl ligand to the metal; upon adequate irradiation, **GS** turns into two different metastable (MS) isomers: the oxygen-bonded isomer (isonitrosyl), called **MS1**, and the sideways-bonded isomer, called **MS2**. Besides photoisomerization, nitrosyl metal complexes can also undergo photorelease of NO and thus display biological activity.[27−31] Despite numerous extensive experimental studies, as well as theoretical investigations, which have afforded a full structural and electronic description of the different isomers,[32−36] the photoisomerization mechanism is still unclear.

The current study focuses on the photoinduced isomerization of the *trans*-$[RuCl(NO)(py)_4](PF_6)_2 \cdot {}^1/_2H_2O$ complex.[37] Figure 1 displays a schematic representation of the structures involved in the photoisomerization process. Upon blue-light irradiation of a single crystal, the **GS** isomer (orange translucent crystal) turns into the **MS1** isomer (green translucent crystal). Subsequent irradiation with near-IR light generates a mixture of **GS** and **MS2** (black crystal); the latter eventually returns to the starting isomer **GS** (Figure 1). Alternatively, **MS1** returns to **GS** upon red-light irradiation.[26] A remarkable conversion of ca. 100% from **GS** toward **MS1** was achieved on a single crystal upon irradiation for 1 h.[24]

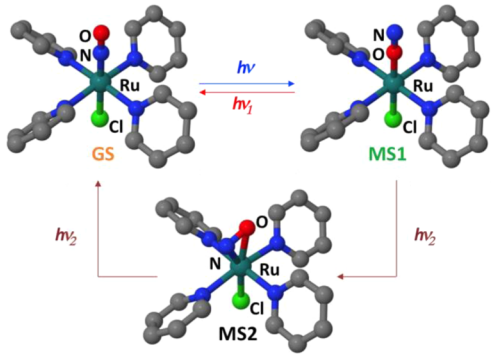

Figure 1. Schematic representations of the linkage isomers of the *trans*-$[RuCl(NO)py_4]^{2+}$ complex in its ground state (**GS**), metastable states (**MS1** and **MS2**), and experimental irradiation conditions (blue, 473 nm; red, 782 nm; dark red, 980 nm).[23−26]

Received: May 4, 2015
Published: August 14, 2015

DOI: 10.1021/acs.inorgchem.5b00998
Inorg. Chem. 2015, 54, 8310−8318

Electronic structure calculations have become an essential tool in the search of new materials and the understanding of their properties. In particular, density functional theory (DFT) and its time-dependent formalism (TDDFT) have been shown to be efficient for the reproduction of UV−vis absorption spectra of metal nitrosyl complexes.[38−40] Besides, DFT has proven to be a powerful method to describe the photoisomerization of ruthenium polypyridine or nitrosyl metal complexes and to propose underlying mechanisms.[41−49] In all of these studies, triplet excited states appear to play a major role; this also holds for the current system. For the first time, complete pathways for the photoinduced linkage isomerization of **GS** toward **MS1** and the reverse photoreaction from **MS1** to **GS** are unveiled in this study.

The Article is organized as follows: First, the ground-state (singlet) potential energy surface (PES) is studied in order to describe a possible thermal isomerization pathway. Second, the TDDFT absorption spectra of the three species are discussed, and the different electronic transitions are characterized. This TDDFT analysis proves to be especially important to rationalize the experimental conditions necessary for the forward and reverse photoisomerizations. Next, the lowest triplet PES with all of the characteristic critical points is reported to discuss the full excited-state adiabatic pathway. Then, singlet−triplet minimum-energy crossing points (MECPs) are discussed in the context of nonradiative deactivation and intersystem crossing (ISC). Finally, all of this information allows us to establish a photoisomerization mechanism for the conversion from **GS** to **MS1** and for the reverse conversion from **MS1** to **GS**.

2. COMPUTATIONAL DETAILS

Gas-phase geometry optimizations of all of the stationary points found on the closed-shell singlet (hereafter called "singlet" for simplicity) and the lowest triplet PES were carried out with the *Gaussian 09* quantum package.[50] Starting from the crystallographic X-ray structures,[24] the isomers **GS** and **MS1** were optimized in C_4 symmetry. DFT was used in order to perform these calculations using the standard hybrid functional B3LYP,[51,52] including Grimme's dispersion correction,[53] with a double-ζ Ahlrichs-type basis set[54] with a p polarization function for the hydrogen atoms, a triple-ζ Ahlrichs-type basis set[54] with one d polarization function for the second- and third-row elements, and for ruthenium a Stuttgart relativistic effective core potential[55] (including 28 core electrons) with its associated basis set[55] and two f and one g polarization functions.[56] After geometry optimizations, vibration frequency analyses were performed at the same level of theory to verify the nature of the stationary points. At the transition state (TS) geometries, steepest-descent (SD) optimizations and subsequent intrinsic reaction coordinate (IRC) calculations were carried out to confirm the connections between the isomers on the singlet and triplet PESs.

In the vicinity of singlet and triplet minima, a search for MECPs has been performed. Optimization of the MECPs was performed with the *ORCA 3.0.2* quantum package[57] at the same level of theory. The UV−vis absorption spectra of **GS**, **MS1**, and **MS2** in acetonitrile[58] were computed using the COSMO[59] solvation model with ORCA, applying TDDFT using the TPSSh[60] functional within the Tamm-Dancoff approximation,[61,62] and the same basis sets as described above. The natural transition orbitals (NTOs)[63] corresponding to the different singlet excited states at the **GS**, **MS1**, and **MS2** geometries were also computed. Complete active-space self-consistent field (CASSCF) plus second-order *n*-electron valence states for multireference perturbation theory (NEVPT2)[64−66] calculations have also been done on the **MS1** state in order to confirm the results of TDDFT calculations in the lowest-energy part of the absorption spectrum (six electrons and six orbitals; see Table S18). For the reverse photoisomerization **MS1** → **GS**, two-photon absorption (TPA) was envisaged for **MS1** and **MS2**. The TPA probability was computed using GAMESS-US[67] within the formalism presented in the work of Zahariev et al.[68] For the final results, eq 93 from the work of Friese et al.[69] has been used. Natural bond orbital (NBO) analyses are a powerful tool for the study of chemical bonding. This kind of analysis was performed at the optimized geometries of **GS**, **MS1**, and **MS2**. It was performed with *NBO 6*,[70,71] which is directly accessible from ORCA.

3. RESULTS

3.1. Singlet PES. The three *trans*-$[RuCl(NO)(py)_4]^{2+}$ isomers, **GS**, **MS1**, and **MS2**, were optimized, and the computed geometries were compared to the experimental data (Table 1). As pointed out before,[25] the geometries of the three isomers are well reproduced with B3LYP. From a structural point of view, the four pyridine ligands appear as spectator ligands because their spatial arrangement in the three isomers is very similar. It is important to remind everyone that, as mentioned in ref 24, the reduced data set available for **MS2** did not permit a perfect refinement of the X-ray crystallographic structure. Thus, the experimental bond lengths might not be fully reliable, in particular the N−O distance, which is reported to be only 1.08 Å (too short for a N−O bond length). A sideways-bonded NO ligand should indeed see its N−O distance increase, as was obtained by DFT. Further information on the optimized structures can be found in the Supporting Information (Tables S1−S3). The energetic ordering of the isomers also perfectly fits the experimental data.

Table 1. Selected Geometrical Parameters (Distances in Å and angles in deg) for the Three Isomers in Their Singlet and Lowest Triplet States

	parameter	X-ray data[24]	singlet state	triplet state
GS	$Ru-N_{NO}$	1.755	1.745	1.975
	$Ru-O_{NO}$		2.886	2.901
	N−O	1.146	1.141	1.155
	Ru−Cl	2.321	2.317	2.290
	$Ru-N_{py}$	2.107[a]	2.139[b]	2.132[a]
	∠Ru−N−O	178.3	180.0[b]	134.2
MS2	$Ru-N_{NO}$	1.921	1.926	2.148
	$Ru-O_{NO}$	2.144	2.163	2.099
	N−O	1.08	1.177	1.216
	Ru−Cl	2.305	2.302	2.249
	$Ru-N_{py}$	2.101[a]	2.147[a]	2.144[a]
	∠Ru−N−O	87.3	84.7	71.1
MS1	$Ru-N_{NO}$		2.991	3.092
	$Ru-O_{NO}$	1.863	1.854	2.169
	N−O	1.140	1.137	1.159
	Ru−Cl	2.278	2.278	2.252
	$Ru-N_{py}$	2.097[a]	2.128[b]	2.121[a]
	∠Ru−N−O		0.0[b]	30.2

[a]Mean value for the four different $Ru-N_{py}$ distances. [b]Optimized in C_4 symmetry.

Location and subsequent optimization of the TSs connecting the three isomers, along with IRC calculations, allowed full characterization of a possible thermal isomerization pathway. Following this procedure, the singlet PES was determined along the isomerization reaction coordinate, with $^1TS_1$ connecting the **GS** and **MS2** isomers and $^1TS_2$ connecting the **MS2** and **MS1** isomers (Supporting Information, Tables S4 and S5 and Figures S5 and S6). The results are presented in Figure 2. Compared to previous work,[23] the trend is well reproduced.

DOI: 10.1021/acs.inorgchem.5b00998
Inorg. Chem. 2015, 54, 8310−8318

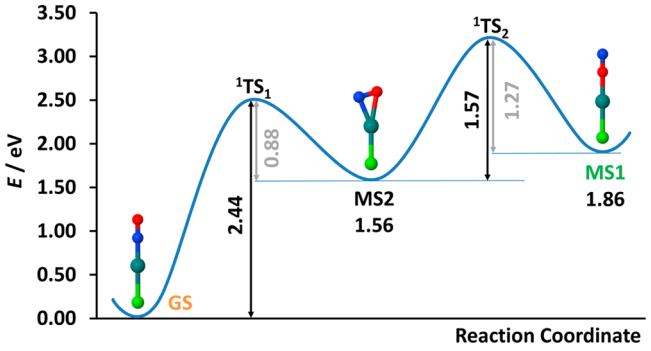

Figure 2. Singlet ground-state potential energy profile of *trans*-$[RuCl(NO)(py)_4]^{2+}$ along the isomerization reaction coordinate.

By analogy with the photoisomerizable iron(II) nitrosyl complexes, the first step of the thermal isomerization pathway would consist of the conversion of **GS** to **MS2**, 1.56 eV (150.5 kJ/mol) higher in energy, with a highly unfavorable 2.44 eV energy barrier (235.4 kJ/mol). With a sideways-bound NO ligand, the **MS2** geometry roughly corresponds to half of the geometric deformation between **GS** and **MS1**, and the nitrogen atom is much closer to the ruthenium atom than the oxygen atom (Table 1). The second step from **MS2** to **MS1** is also kinetically highly unfavorable [barrier of 1.57 eV (151.5 kJ/mol)] but only slightly thermodynamically unfavorable [**MS1** lies 0.30 eV (28.9 kJ/mol) higher than **MS2**]. Thus, from a kinetic and thermodynamic point of view, the **GS** → **MS1** isomerization cannot be achieved on the singlet state PES.

The reverse pathway from **MS1** to **GS** is thermodynamically favorable (exothermic), and from a kinetic point of view, it is more favorable than the forward process because the energy barriers are reduced: 1.27 eV (122.5 kJ/mol) from **MS1** to **MS2** and 0.88 eV (84.9 kJ/mol) from **MS2** to **GS**. Thus, the thermal isomerization pathway from **MS1** to **GS** is globally more favorable than the linkage isomerization from **GS** to **MS1** but would remain challenging.

In an attempt to rationalize the energetic profile shown in Figure 2, an NBO analysis was undertaken. A second-order perturbation theory analysis of the Fock matrix in the NBO basis set allows a quantitative analysis, in terms of stabilizing energies gained upon electron delocalization between donors and acceptors, and a qualitative analysis based on interacting fragments in terms of two-center bonds and three-center four-electron (3c-4e) hyperbonds. Table 2 reports the main results from this NBO analysis.

The energetic ordering of the three isomers is perfectly mirrored in the total delocalization energies. The energy gaps that appear on Figure 2 are also very well reproduced. From this analysis, **GS** is expected to be much more stabilized than **MS2** and **MS1**. **MS1** is expected to be slightly less stabilized than **MS2**. In terms of interacting fragments, **GS** and **MS2** are composed of two fragments, while **MS1** is described by one fragment only because one bonding orbital is found between the ruthenium and nitrogen atoms. Along the forward pathway, the largest activation barrier is associated with the disappearance of two highly stabilizing hyperbonds, in particular because of the tilting of the nitrogen lone pair and the loss of Cl−Ru−N linearity (from **GS** to **MS2**). When the Ru−N bond of **MS2** is broken (from **MS2** to **MS1**), a large activation barrier is also found. In the **MS1** isomer, it should be noticed that the (N)O → RuCl interaction is much weaker than the (O)N → RuCl interaction in **GS**. Along the reverse pathway, slightly smaller activation barriers are associated with the disappearance of one hyperbond (from **MS1** to **MS2**) or one bond (from **MS2** to **GS**). It can be seen that in this case the NBO analysis explains perfectly the relative positions of the three isomers as well as the energetic barriers between them.

3.2. Absorption Spectra of GS, MS1, and MS2.

Irradiation of **GS** with blue light at 473 nm happens to produce the largest amount of **MS1**. We will return to this point later (section 4.1). On the way back, irradiation with red light at several wavelengths (658, 782, and 808 nm)[26] can be used to generate **GS** from **MS1**.

As can be observed in Figure 3, isomers **GS** and **MS2** present absorption bands in the region from 400 to 500 nm and

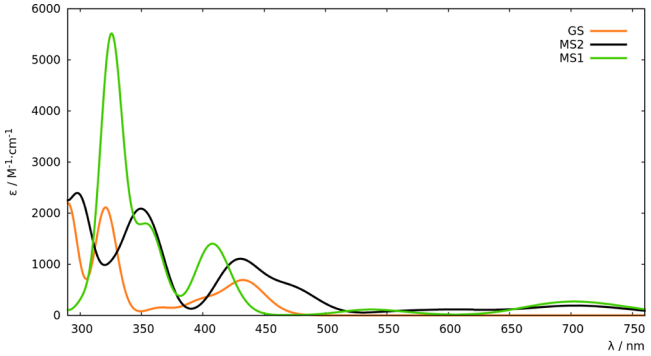

Figure 3. TDDFT spectra of the three linkage isomers of *trans*-$[RuCl(NO)(py)_4]^{2+}$ computed in acetonitrile.

isomers **MS1** and **MS2** show similar absorption bands in the 600−750 nm spectral region. It should be noted that the extinction coefficients of the bands in those regions are quite small compared to those of polypyridyl ruthenium complexes. This is one of the reasons why the experimental irradiation times needed to achieve the photoisomerization are on the order of tens of minutes. In Table 3, the nature, absorption wavelengths, and oscillator strengths of the main transitions are summarized (NTO for the selected states can be found in Tables S15−S17).

Experimentally, only the absorption of pure **GS** is available in solution (450 nm).[58] In order to reproduce this spectrum, it is necessary to take into account solvent effects (Figures S1−S4).

Table 2. Delocalization Energies (kJ/mol; Donation and Backdonation Are Defined with Respect to the Metal Center), Nature of the Fragments, and Number of Bonds and Hyperbonds

	delocalization energy				
	donation	backdonation	sum	fragments	bonds/hyperbonds
GS	1367 (ON → RuCl)	744 (RuCl → NO)	2111	[Cl−Ru]/[NO]	0/3
MS2	995 (ON → RuCl)	217 (RuCl → NO)	1212	[Cl−Ru−NO]	1/1
MS1	693 (NO → RuCl)	267 (RuCl → ON)	960	[Cl−Ru]/[ON]	0/2

DOI: 10.1021/acs.inorgchem.5b00998
Inorg. Chem. 2015, 54, 8310−8318

Table 3. Selected TDDFT States near the Spectral Irradiation Wavelengths (i.e., in the 400−500 and 600−1100 nm Ranges) Computed in Acetonitrile for the Three Isomers in Their Singlet States (Oscillator Strength Threshold 10^{-3})

	state	wavelength/nm	f_{osc}	nature
GS	S_1, S_2	434	0.0031	Ru(d) → Ru(d)NO(π^*)
	S_6, S_7	402	0.0010	py(π) → Ru(d)NO(π^*)
MS2	S_1	706	0.0017	Cl(p)Ru(d) → Ru(d)NO(π^*)
	S_6	478	0.0016	Cl(p)Ru(d)NO(π^*) → Ru(d)NO(π^*) py(π)Ru(d) → Cl(p)Ru(d)NO(π^*)
	S_7	476	0.0020	Cl(p)Ru(d) → Ru(d)NO(π^*) Cl(p)Ru(d) NO(π^*) → Cl(p)Ru(d)NO(π^*)
	S_{10}	450	0.0012	py(π) → Cl(p)Ru(d)NO(π^*)
	S_{11}	436	0.0028	Cl(p)Ru(d)py(π) → Ru(d)NO(π^*)
	S_{12}	433	0.0021	Cl(p)Py(π) → Cl(p)Ru(d)NO(π^*)
	S_{13}	427	0.0019	Cl(p)Ru(d)py(π) → Ru(d)NO(π^*)
	S_{15}	417	0.0030	Cl(p)py(π) → Ru(d)NO(π^*)
MS1	S_1, S_2	703	0.0013	Ru(d) → Ru(d)ON(π^*)
	S_{17}	408	0.0043	Cl(p)py(π) → Ru(d)ON(π^*)
	S_{18}, S_{19}	408	0.0043	py(π) → Ru(d)ON(π^*)

In these conditions, the lowest-energy absorption band is computed at 434 nm (416 nm without solvent). The 434 nm band in the spectrum of the **GS** isomer (Table 3) corresponds to two degenerate metal-to-ligand charge-transfer (MLCT) transitions from a Ru(d_{xy}) orbital to antibonding RuNO (d_{xz}−π_x* and d_{yz}−π_y*) molecular orbitals (MOs).[72] At higher energies in the spectral region of interest, the two other states, S_6 and S_7, correspond to transitions from pyridyl MOs to the Ru−NO MOs described before.

The **MS2** spectrum displays its lowest-energy band at λ_{max} = 706 nm (Figure 3). The **MS2** isomer presents a band similar to that of **GS** in the region between 400 and 500 nm. This is crucial, as shown in the description of the photoisomerization mechanism. At the experimental irradiation wavelength (473 nm), **MS2** is the most efficient absorber of the three isomers. The excitation wavelength that produces the largest amount of **MS1** is 473 nm, which corresponds to a compromise between the absorptions of **GS** and **MS2**.

The **MS1** isomer shows a band at the same position and intensity as **MS2** at 703 nm. It should be noted that, upon transposition of the 0.1 eV shift found for **GS** between theory and experiment, **MS1** does not absorb at the experimental irradiation wavelength (473 nm).

3.3. Lowest Triplet PES. The lowest triplet PES was explored in order to investigate a possible adiabatic N → O linkage photoisomerization on this surface, similarly to ruthenium sulfoxides.[41−45,73,74] The singly occupied natural orbitals, geometries, spin densities, and other relevant information on the three minima can be found in Tables S6−S8. Starting from the singlet optimized structures, three different stationary points corresponding to three different minima were identified. These minima were labeled according to their affiliation with their corresponding closed-shell isomer: ^{3}**GS**, ^{3}**MS2**, and ^{3}**MS1**. On the basis of Mulliken spin densities, these triplet states can be considered as standard MLCT states. It is worth noticing that, in contrast with polypyridyl ruthenium complexes, no triplet metal-centered states (^{3}MC) have been identified for this system on the lowest triplet PES.[43,45,73,74]

The lowest triplet state minima have been compared with their parent singlet geometries (Table 1) in order to highlight the main geometrical differences. It is remarkable that the Ru−N−O (or its homologous Ru−O−N for the **MS1**/^{3}**MS1** couple) bond angle bends from 180° (in **GS** and **MS1**) to 134° (in ^{3}**GS** and ^{3}**MS1**). Furthermore, the triplet states exhibit an elongated bond to the nitrosyl or isonitrosyl ligand, from 1.745 Å (**GS**) to 1.975 Å (^{3}**GS**) and from 1.854 Å (**MS1**) to 2.169 Å (^{3}**MS1**). Thus, for both the forward and reverse photoisomerizations, population of the triplet state initiates the rotation of the NO ligand.

In the Ru−NO → Ru−ON isomerization process (**GS** → **MS1**), the key geometrical change must involve a step where Ru−N < Ru−O becomes Ru−O < Ru−N. This key step is observed with the population of ^{3}**MS2**, whose geometry perfectly reflects this inversion (Table 1). From a structural point of view, it seems more favorable to go from one triplet to the other, rather than from one singlet to the other, because the changes in the Ru−N−O angles in the triplet state are smaller. The location and optimization of the TSs, followed by IRC calculations, is shown in Figure 4, with $^3TS_1$ connecting the ^{3}**GS** and ^{3}**MS2** minima and $^3TS_2$ connecting ^{3}**MS2** and ^{3}**MS1** minima (further information can be found in Tables S9 and S10 and Figures S7 and S8).

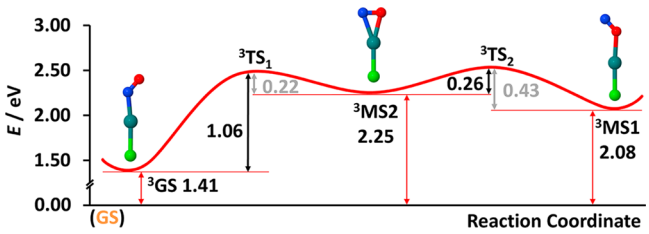

Figure 4. Lowest triplet potential energy profile of *trans*-$[RuCl(NO)(py)_4]^{2+}$ along the photoisomerization reaction coordinate.

The energy gaps between the first two minima are smaller in the triplet state case (^{3}**GS** → ^{3}**MS2**: 0.84 eV, 81.1 kJ/mol) than in the singlet state case (**GS** → **MS2**: 1.56 eV, 150.5 kJ/mol). With the ^{3}**MS2** state being the highest of all triplet minima, the second step is now thermodynamically favorable (−0.17 eV, 16.4 kJ/mol), while it was unfavorable on the singlet state PES (+0.30 eV, 28.9 kJ/mol).

The energy barriers encountered on the triplet PES are all reduced with respect to the singlet PES. However, the barrier found between ^{3}**GS** and ^{3}**MS2** (1.06 eV, 102.3 kJ/mol) is still large, but once ^{3}**MS2** is reached, the progression of the reaction toward ^{3}**MS1** is, from a thermodynamic and a kinetic (0.26 eV,

DOI: 10.1021/acs.inorgchem.5b00998
Inorg. Chem. 2015, 54, 8310−8318

25.1 kJ/mol) point of view, favorable. Thus, the reaction would be easier on the lowest triplet PES than on the singlet PES.

The reverse pathway from ^{3}**MS1** to ^{3}**GS** is globally more favorable than the forward one, with an initial ^{3}**MS1** → ^{3}**MS2** barrier of 0.43 eV (41.5 kJ/mol) and a second ^{3}**MS2** → ^{3}**GS** barrier of 0.22 eV (21.2 kJ/mol). The backreaction ^{3}**MS1** → ^{3}**GS** is exothermic; ΔE = −0.67 eV (−64.6 kJ/mol).

3.4. Singlet−Triplet MECPs. In order to discuss possible nonadiabatic relaxation pathways, we have also searched the MECPs between the lowest triplet PES and the singlet state PES. This kind of relaxation through MECPs is decisive in the photoisomerization mechanism of ruthenium sulfoxide and phosphinidene oxide complexes.[43−45] The size of the singlet−triplet spin−orbit coupling constant, about 1000 cm^{-1},[49,75] is sufficient to ensure that ISC will occur at these crossing points. Four MECPs between the singlet and triplet PESs were found and are shown in Figure 5 (the geometries, gradients, triplet

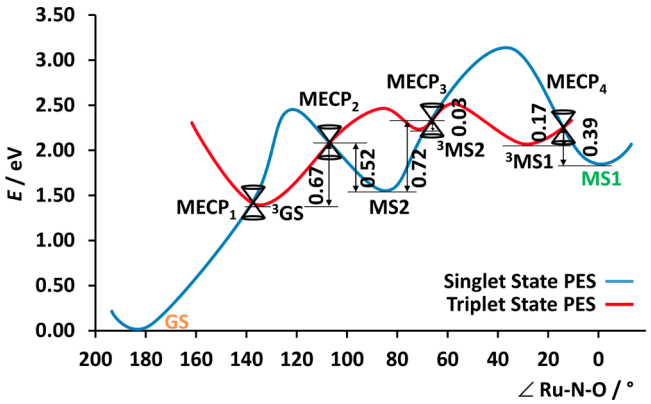

Figure 5. Energy profile showing the singlet−triplet MECPs versus the Ru−N−O angle of *trans*-[RuCl(NO)(py)$_4$]$^{2+}$. The blue line represents the lowest-energy reaction path of the closed-shell singlet state along the photoizomerization process. The red line represents the lowest triplet state energy path along the photoizomerization process. Triplet−singlet funnels are represented by double-cone pictograms.

electronic structures, and relaxation pathways at these MECPs can be found in Tables S11−S14 and Figures S9−S12). The energy is plotted against the Ru−N−O angle, which was selected as a relevant reaction coordinate for the photoisomerization process.

The first MECP found, MECP$_1$, is almost similar in energy and geometry to ^{3}**GS**. MECP$_2$ is located between the geometries of the ^{3}**GS** and **MS2** species, 0.67 eV (64.6 kJ/mol) higher in energy than ^{3}**GS**. This MECP is very important because it affords a way to go from ^{3}**GS** to **MS2** at a reasonable cost. MECP$_3$ is almost similar in energy and geometry to ^{3}**MS2**. Finally, MECP$_4$ allows the ISC between ^{3}**MS1** and **MS1**, i.e., the population of the final photoisomerization product, **MS1**. It is easily accessible from ^{3}**MS1** (0.17 eV, 16.4 kJ/mol) and has an intermediate geometry between **MS1** and ^{3}**MS1** (especially in terms of the Ru−O distance and Ru−O−N angle). As will be explained in the discussion, MECP$_4$ is important for both the forward and reverse isomerizations.

4. DISCUSSION

Before a discussion about the photoisomerization mechanisms of the *trans*-[RuCl(NO)py$_4$]$^{2+}$ system is presented in detail, three points have to be noted to describe this peculiar system:

(i) From a structural point of view, the **MS2** geometry is an inevitable stopover and plays a central role in the mechanism, in the both forward and reverse directions. In addition, we have seen that the absorption properties of **MS2** were partly overlapping those of **GS** (in the blue region) and partly overlapping those of **MS1** (in the red region). This property makes **MS2** the cornerstone of this photoisomerization.

(ii) The second remarkable specificity of this system is that, during the rotation of the NO fragment, two important regions of the PES exhibit the high-spin state (triplet states) as being more stable than the low-spin state (closed-shell singlet states). This is reminiscent of the physical properties of iron(II) magnetic compounds where spin crossover commonly occurs.

(iii) Our initial working hypothesis is that the photoisomerization occurs on the lowest triplet PES. However, on the basis of the following calculations, we have envisaged the significant intervention of higher excited states (noted as T$_n$ hereafter) in the mechanism, which avoid invoking thermodynamically uphill steps.

4.1. Mechanism for the Forward Isomerization (GS → MS1). The forward isomerization is performed by irradiation of the single crystal with λ = 473 nm at ca. 100 K for 1 h.[24] The **GS** → **MS1** photoisomerization can be viewed as a two-step sequence (**GS** → **MS2** followed by **MS2** → **MS1**), in which **MS2** is an essential intermediate displaying an η^2 geometry. The corresponding mechanism is schematically presented in Figure 6.

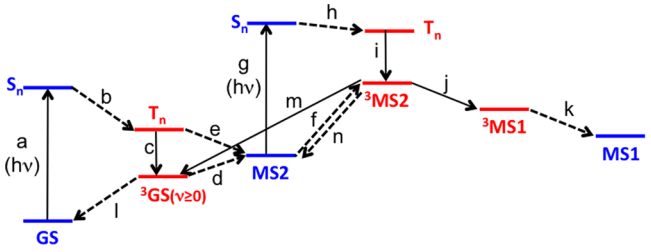

Figure 6. Schematic depiction of the major events involved in the photoisomerization mechanism from **GS** to **MS1**. The various steps that result in population of the **MS1** state are labeled sequentially (a−k). Solid arrows are used when states of the same multiplicity are involved, and dashed arrows are used otherwise. The singlet states are in blue and the triplet states in red.

Step 1: GS → MS2. Following photoexcitation (elementary step a in Figure 6), ^{3}**GS** is populated (steps b and c). The a, b, and c sequence is extremely well documented both experimentally and, more recently, theoretically, on the ruthenium complexes.[49,76,77] S$_n$ refers to the lowest most absorbing singlet state. T$_n$, which is coupled by spin−orbit coupling with S$_n$, should be more or less degenerate with S$_n$ and, furthermore, should be built on a determinant having one orbital orthogonal to the S$_n$ determinant. Step c is the internal conversion from T$_n$ to the lowest triplet state, i.e., ^{3}**GS**. From ^{3}**GS**, ISC through MECP$_2$ (step d) populates **MS2** in its ground state. This step d involves an important change in the Ru−N−O angle (from 134.2° to 84.7°) and in the Ru−O distance (from 2.90 to 2.16 Å). Assuming a full thermal relaxation to ^{3}**GS**(ν=0), the activation energy to reach MECP$_2$ amounts to 0.67 eV (64.6 kJ/mol). Alternatively, if ^{3}**GS** is populated in high vibrational states, i.e., ^{3}**GS** (ν>0), then the 0.67 eV value is just an upper limit of this activation energy. In addition, a direct connection between T$_n$ and **MS2** has also

DOI: 10.1021/acs.inorgchem.5b00998
Inorg. Chem. 2015, 54, 8310−8318

been considered (step e). In particular, two triplets states, which lie 0.47 and 0.70 eV (45.3 and 67.5 kJ/mol) above ^{3}**GS** (at the ^{3}**GS** geometry), are perfect candidates to populate **MS2** and would avoid the system to fall in the ^{3}**GS** potential well. It is even possible that these triplet states undergo ISC to MS2, but this point was not addressed in this work.

*Step 2: **MS2** → **MS1***. To continue the isomerization process from **MS2** and literally to be dragged out of the **MS2** potential well, the system has to be excited to the ^{3}**MS2** state. As seen in the geometries (Table 1), the **MS2** → ^{3}**MS2** step is crucial to switch in favor of the isonitrosyl coordination. Population of ^{3}**MS2** can be achieved either by overcoming a 0.73 eV (70.4 kJ/mol) barrier to reach $MECP_3$ (step f) or much more probably by absorption of another blue photon (step g) and subsequent relaxation to ^{3}**MS2** (steps h and i). Indeed, with such energy barriers to reach $MECP_2$ or $MECP_3$ that surround **MS2**, the system should be trapped in the **MS2** isomer long enough to be detected by a color change of the crystal. However, the irradiated crystal goes directly from orange to green. Hence, before the **MS2** isomer can be detected, it is depopulated by the absorption of a second photon. As seen in its absorption spectrum, **MS2** absorbs strongly at the experimental excitation wavelength. Thus, once the system reaches the **MS2** isomer, it absorbs a blue photon and relaxes preferentially to ^{3}**MS2** (**GS** → **MS1** photoisomerization completed in 1 h) versus relaxing to ^{3}**GS**.

The next step (^{3}**MS2** → ^{3}**MS1** via $^3TS_2$, step j) involves mainly a dramatic change in the Ru−N−O angle (from 71.1° to 30.2°) and a marked shortening of the N−O distance (from 1.216 to 1.159 Å). The last step of the photoisomerization (^{3}**MS1** → **MS1**, step k) consists of an ISC through $MECP_4$, with a small energy barrier of 0.17 eV (16.4 kJ/mol). The main coordinate involves a change in the Ru−N−O angle from 30.2° to 0.0°.

*Pitfalls along the **GS** → **MS1** Path*. Depending on their location and depending on which side they are accessed from, MECPs can act as either reactive or quenching funnels for the photoisomerization process. The first pitfall (step l) is encountered very close to ^{3}**GS**, where $MECP_1$ takes the system back to the starting point. This relaxation back to **GS** is the most probable path because it only involves spin change (almost no energy barrier). This is an important trap that would make the photoisomerization quite inefficient. The second pitfall is that the ^{3}**MS2** state can either go forward to ^{3}**MS1** (as seen before) or return to ^{3}**GS** (step m) with similar barriers (0.26 vs 0.22 eV). In addition, in the vicinity of ^{3}**MS2** lies $MECP_3$, which allows the system to return to **MS2** (step n).

It is noteworthy that, experimentally, photoisomerization is achieved using a monochromatic excitation only because **GS** and **MS2** absorb at the same wavelength. This photoisomerization fulfills the general scheme proposed by Ishikawa and Tanaka,[78] where the absorption of a photon weakens the M−NO bond and crucial crossings are found between the singlet and triplet excited-state surfaces.

4.2. Mechanism for the Reverse Isomerization (MS1 → GS). The oxygen-bound **MS1** isomer is formed upon blue-light irradiation at low temperature, ca. 100 K. It is stable in the dark, but degradation is observed upon heating and upon red-light irradiation. Indeed, the **MS1** → **GS** transformation is achieved experimentally either by irradiation at 782 nm for 30 min[26] or by irradiation at 980 nm for 30 min to form a ca. 1:1 mixture of **MS2**/**GS**, which can eventually become the pure **GS** isomer upon heating.[24] The corresponding mechanisms have been studied separately and are schematically presented in Figures 7 and 8, respectively.

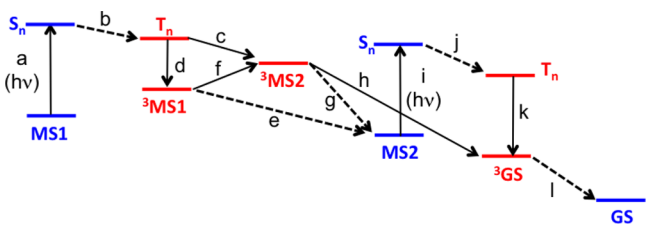

Figure 7. Schematic depiction of the major events involved in the photoisomerization mechanism from **MS1** to **GS** with red light. The various steps that result in the population of the **GS** state are labeled sequentially (a–l). Solid arrows are used when states of the same multiplicity are involved, and dashed arrows are used otherwise. The singlet states are in blue and the triplet states in red.

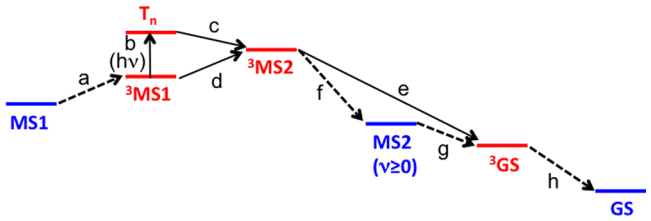

Figure 8. Schematic depiction of the major events involved in the photoisomerization mechanism from **MS1** to **GS** with near-IR light. The various steps that result in the population of the **GS** state are labeled sequentially (a–h). Solid arrows are used when states of the same multiplicity are involved, and dashed arrows are used otherwise. The singlet states are in blue and the triplet states in red.

- *Red-Light Excitation (Figure 7)*. In the red spectral range, **MS1** (and also **MS2**) shows a broad absorption band (650–800 nm) centered at 705 nm (Figure 3). Starting from **MS1**, the initial step of the mechanism consists of the absorption of a photon (step a in Figure 7). Similarly to the previous case, S_n undergoes ISC to T_n, which may directly convert into ^{3}**MS2** (step c). Which T_n converts into ^{3}**MS2** is an open question because we dispose of two other triplets [0.50 and 0.55 eV (48.2 and 53.1 kJ/mol) higher in energy than ^{3}**MS1** at its proper geometry] that could populate ^{3}**MS2**. If the system relaxes to ^{3}**MS1** (step d), then there are two possibilities to depopulate this state: (i) by population of **MS2** through $MECP_3$ (step e); (ii) by population of ^{3}**MS2** via $^3TS_2$ (step f). If the system reaches ^{3}**MS2**, it can either relax to **MS2** through $MECP_3$ (step g) or relax to ^{3}**GS** through $^3TS_1$ (step h). In the latter case, only one photon is needed to complete the reaction.

If the system reaches **MS2**, it can absorb a red photon (step i) because both **MS2** and **MS1** absorb at the excitation wavelength. This is consistent with the impossibility of observing **MS2** when irradiation is performed at 782 nm; i.e., **MS2** is simultaneously produced and used; hence, it does not accumulate.[26] As described before, depending on the excitation wavelength, excitation of **MS2** to an excited singlet S_n can lead to the population of either ^{3}**MS2** or ^{3}**GS**. The very fact that, at the end of the process, a pure **GS** orange crystal is obtained implies that, at this wavelength (red light), the system evolves mainly to ^{3}**GS** (steps j and k). The final step from ^{3}**GS** to **GS** involves relaxation through $MECP_1$ (step l) via an efficient ISC with almost no energy barrier.

DOI: 10.1021/acs.inorgchem.5b00998
Inorg. Chem. 2015, 54, 8310−8318

In summary, there are two pathways for the reverse **MS1** → **GS** photoisomerization: one that involves the absorption of only one photon, which avoids formation of the **MS2** isomer, and a second one consisting of the sequential absorption of two photons by populating and depopulating the **MS2** isomer.

- *IR-Light Excitation (Figure 8).* IR light has been used to induce the stepwise photoisomerization from **MS1** to **GS** via **MS2**, with the total disappearance of **MS1** being observed after 30 min of irradiation.[24] A 1:1 mixture of **GS** and **MS2** is obtained, according to X-ray diffraction and IR spectroscopy,[23] which slowly evolves into a crystal of **GS** after a further 7 h of irradiation or just by an increase in the temperature.

As seen in the TDDFT spectrum of **MS1** (Figure 3), there is no absorption band in this region; this has been confirmed by using several functionals (B3LYP,[51,52] PBE0,[79] TPSSh,[60] X3LYP,[80] ωB97X,[81] and LC-PBE[82,83]) and also by CASSCF/NEVPT2[64−66] calculations, which can be found in the Supporting Information (Tables S18 and S19). Thus, IR light is not capable of causing electronic excitations of **MS1**, and thus other explanations must be found to justify the disappearance of **MS1**. TPA cannot be excluded because many excited states fall in the suitable range. Alternatively, given that **MS1** can be thermally depopulated and by analogy with iron(II) spin-crossover compounds,[84] one can propose that a fraction of **MS1** exists as ^{3}**MS1**. Depopulation of ^{3}**MS1** by IR-light excitation ensures the gradual consumption of **MS1**.

In the hypothesis of a TPA, **MS1** would be excited to higher singlet states, which by ISC could populate the ^{3}**MS1** state. Indeed, the ca. 1000 nm excitation wavelength (corresponding to a virtual excitation of 500 nm) matches several excited states of **MS1**. We have calculated the TPA cross sections for these states, but these cross sections lie around 10^{-4} GM, which is too low to yield efficient excitations. Furthermore, calculations on **MS2** show similar cross sections. Hence, if **MS1** excitation (by TPA) was sufficient, **MS2** would be consumed as soon as produced and, thus, it could not be observed, in contrast to experimental evidence. Thus, TPA can be ruled out.

In the second hypothesis, which has not yet been experimentally proven, the system can partially exist as ^{3}**MS1** (step a in Figure 8) thanks to spin−orbit coupling and a low activation energy (0.38 eV). Interestingly, two transitions are found in the ^{3}**MS1** TDDFT calculation, at 933 and 1396 nm, near the experimental irradiation wavelengths (980 and 1064 nm). Thus, absorption from ^{3}**MS1** takes the system to higher electronic triplet states T_n (step b), and then the system can relax to ^{3}**MS2** via internal conversion (step c). Alternatively, ^{3}**MS1** can also populate ^{3}**MS2** via $^3TS_2$ (step d), but with this step being thermodynamically uphill, it is certainly less probable than step c. Once the system gets to ^{3}**MS2**, it can either relax to ^{3}**GS** through $^3TS_1$ (step e) or easily relax to **MS2** through $MECP_3$ (step f) (this explains why **MS2** is always observed as a blend of **GS** and **MS2**). The **MS2** isomer does not absorb in the IR region, and thus it is trapped long enough to be observed. This is fully consistent with the fact that, experimentally, this is the only way to observe the **MS2** isomer.

From **MS2**, given that the system does not absorb IR light (and TPA is not efficient enough), it can only relax to ^{3}**GS** through $MECP_2$ (step g) with a barrier of 0.52 eV (50.2 kJ/mol) for **MS2**(ν=0). Finally, the last step of the mechanism consists of the ^{3}**GS** → **GS** relaxation via $MECP_1$ (step h).

5. CONCLUSIONS

In this Article, we report a mechanistic study of the reversible nitrosyl linkage photoisomerization in *trans*-$[RuCl(NO)(py)_4]^{2+}$. Three isomers, Ru−NO (**GS**), Ru−η^2-NO (**MS2**), and Ru−ON (**MS1**), are successively populated during the process, which was already well established experimentally. The singlet and triplet PESs show that the forward isomerization, both thermodynamically and kinetically, is unfavorable and thus will necessitate the intervention of two photons. For the reverse photoisomerization with red-light excitation, two pathways coexist: one monophotonic process directly producing GS and one biphotonic process going to **GS** through **MS2**. For the reverse photoisomerization with IR-light excitation, only one species absorbs IR photons and thus only a monophotonic process is operative, yielding both **MS2** and **GS** in the same crystal.

For the forward and reverse mechanisms, the Ru−η^2-NO isomer plays a pivotal role, both optically and structurally, for the second photon absorption: (i) its absorption spectrum overlaps that of **GS** in the blue region and that of **MS1** in the red region, which is a compulsory condition for the forward and backward photoisomerizations to proceed; (ii) its excitation allows the system to go past the tipping point toward **MS1** because Ru−O is shorter than Ru−N in ^{3}**MS2**. It should also be noted that the singlet and triplet PESs are highly entangled, which allows several spin changes along the reaction pathway. Furthermore, in certain regions of the PES, it is the triplet state that is the true ground state.

In contrast with ruthenium sulfoxide complexes, for which metal-centered states play a crucial role because large geometric reorganizations are required,[43,45,73,74] the proposed photoisomerization mechanisms for this system only involve moderately distorted triplet states of MLCT nature.

Besides linkage photoisomerization, metal nitrosyl complexes are promising candidates for NO photorelease. Understanding the factors controlling the competition between NO isomerization and NO release will be very challenging. Approaches that combine static and dynamic studies[49] could bring further insight into the mechanisms involved in the versatile photosensitivity of ruthenium nitrosyl complexes.

■ ASSOCIATED CONTENT

Supporting Information

The Supporting Information is available free of charge on the ACS Publications website at DOI: 10.1021/acs.inorgchem.5b00998.

Tables S1−S10 for Cartesian coordinates, energies, and orbitals of all of the optimized stationary points, Tables S11−S14 for structures of MECPs, Figures S1−S4 for computed absorption spectra with NTO analysis (Tables S15−S17), Table S18 for active-space orbitals of the **MS1** CASSCF(6,6) calculation, Figures S5−S8 for IRC calculations, and Figures S9−S12 for SD optimizations from the four MECPs found (PDF)

■ AUTHOR INFORMATION

Corresponding Author

*E-mail:Heully@irsamc.ups-tlse.fr.

Notes

The authors declare no competing financial interest.

DOI: 10.1021/acs.inorgchem.5b00998
Inorg. Chem. 2015, 54, 8310−8318

■ ACKNOWLEDGMENTS

This work was granted access to the HPC resources of CALMIP supercomputing center under the allocation 2014-[1133]. The authors thank the anonymous reviewer 2 for his valuable comments and suggestions to improve the quality of the paper.

■ REFERENCES

(1) Hauser, U.; Oestreich, V.; Rohrweck, H. D. Z. *Z. Phys. A: At. Nucl.* **1977**, *280*, 17.
(2) Hauser, U.; Oestreich, V.; Rohrweck, H. D. Z. *Z. Phys. A: At. Nucl.* **1977**, *280*, 125.
(3) Pressprich, M. R.; White, M. A.; Vekhter, Y.; Coppens, P. *J. Am. Chem. Soc.* **1994**, *116*, 5233−5238.
(4) Delley, B.; Schefer, J.; Woike, T. *J. Chem. Phys.* **1997**, *107*, 10067−10074.
(5) Boulet, P.; Buchs, M.; Chermette, H.; Daul, C.; Gilardoni, F.; Rogemond, F.; Schläpfer, C. W.; Weber, J. *J. Phys. Chem. A* **2001**, *105*, 8991−8998.
(6) Boulet, P.; Buchs, M.; Chermette, H.; Daul, C.; Furet, E.; Gilardoni, F.; Rogemond, F.; Schläpfer, C. W.; Weber, J. *J. Phys. Chem. A* **2001**, *105*, 8999−9003.
(7) Chacón Villalba, M. E.; Güida, J. A.; Varetti, E. L.; Aymonino, P. J. *Inorg. Chem.* **2003**, *42*, 2622−2627.
(8) Lee, J.; Kovalevsky, A. Y.; Novozhilova, I. V.; Bagley, K. A.; Coppens, P.; Richter-Addo, G. B. *J. Am. Chem. Soc.* **2004**, *126*, 7180−7181.
(9) Novozhilova, I. V.; Coppens, P.; Lee, J.; Richter-Addo, G. B.; Bagley, K. A. *J. Am. Chem. Soc.* **2006**, *128*, 2093−2104.
(10) Lynch, M. S.; Cheng, M.; Van Kuiken, B. E.; Khalil, M. *J. Am. Chem. Soc.* **2011**, *133*, 5255−5262.
(11) Gütlich, P.; Garcia, Y.; Woike, T. *Coord. Chem. Rev.* **2001**, *219-221*, 839−879.
(12) Coppens, P.; Novozhilova, I.; Kovalevsky, A. *Chem. Rev.* **2002**, *102*, 861−884.
(13) Ford, P. C.; Wecksler, S. *Coord. Chem. Rev.* **2005**, *249*, 1382−1395.
(14) Bitterwolf, T. E. *Coord. Chem. Rev.* **2006**, *250*, 1196−1207.
(15) Fomitchev, D. V.; Coppens, P. *Inorg. Chem.* **1996**, *35*, 7021−7026.
(16) Fomitchev, D. V.; Coppens, P.; Li, T.; Bagley, K. A.; Chen, L.; Richter-Addo, G. B. *Chem. Commun.* **1999**, *19*, 2013−2014.
(17) Da Silva, S. C.; Franco, D. W. *Spectrochim. Acta, Part A* **1999**, *55*, 1515−1525.
(18) Gorelsky, S. I.; Lever, A. B. P. *Int. J. Quantum Chem.* **2000**, *80*, 636−645.
(19) Schaniel, D.; Woike, T.; Boskovic, C.; Güdel, H.-U. *Chem. Phys. Lett.* **2004**, *390*, 347−351.
(20) Bitterwolf, T. E. *Inorg. Chem. Commun.* **2008**, *11*, 772−773.
(21) Giglmeier, H.; Kerscher, T.; Klüfers, P.; Schaniel, D.; Woike, T. *Dalton Trans.* **2009**, *42*, 9113.
(22) Zangl, A.; Klüfers, P.; Schaniel, D.; Woike, T. *Dalton Trans.* **2009**, *6*, 1034−1045.
(23) Schaniel, D.; Cormary, B.; Malfant, I.; Valade, L.; Woike, T.; Delley, B.; Krämer, K. W.; Güdel, H.-U. *Phys. Chem. Chem. Phys.* **2007**, *9*, 3717−3724.
(24) Cormary, B.; Malfant, I.; Buron-Le Cointe, M.; Toupet, L.; Delley, B.; Schaniel, D.; Mockus, N.; Woike, T.; Fejfarová, K.; Petříček, V.; Dušek, M. *Acta Crystallogr., Sect. B: Struct. Sci.* **2009**, *65*, 612−623.
(25) Cormary, B.; Ladeira, S.; Jacob, K.; Lacroix, P. G.; Woike, T.; Schaniel, D.; Malfant, I. *Inorg. Chem.* **2012**, *51*, 7492−7501.
(26) Khadeeva, L.; Kaszub, W.; Lorenc, M.; Malfant, I.; Buron-Le Cointe, M. *Submitted*.
(27) Tfouni, E.; Krieger, M.; McGarvey, B. R.; Franco, D. W. *Coord. Chem. Rev.* **2003**, *236*, 57−69.
(28) Pestana, C. R.; Phelippin, D. P. S.; Polizello, A. C. M.; Dorta, D. J.; Uyemura, S. A.; Santos, A. C.; Doro, F. G.; Rodrigues, F. P.; Tfouni, E.; Curti, C. *Nitric Oxide* **2009**, *20*, 24−30.
(29) Melo Pereira, J. C.; Carregaro, V.; Costa, D. L.; Santana da Silva, J.; Cunha, F. Q.; Franco, D. W. *Eur. J. Med. Chem.* **2010**, *45*, 4180−4187.
(30) Tfouni, E.; Truzzi, D. R.; Tavares, A.; Gomes, A. J.; Figueiredo, L. E.; Franco, D. W. *Nitric Oxide* **2012**, *26*, 38−53.
(31) Ford, P. C. *Nitric Oxide* **2013**, *34*, 56−64.
(32) Caramori, G. F.; Frenking, G. *Organometallics* **2007**, *26*, 5815−5825.
(33) Caramori, G. F.; Kunitz, A. G.; Andriani, K. F.; Doro, F. G.; Frenking, G.; Tfouni, E. *Dalton Trans.* **2012**, *41*, 7327.
(34) Andriani, K. F.; Caramori, G. F.; Doro, F. G.; Parreira, R. L. T. *Dalton Trans.* **2014**, *43*, 8792−8804.
(35) Delcey, M. G.; Freitag, L.; Pedersen, T. B.; Aquilante, F.; Lindh, R.; González, L. *J. Chem. Phys.* **2014**, *140*, 174103.
(36) Freitag, L.; Knecht, S.; Keller, S. F.; Delcey, M. G.; Aquilante, F.; Bondo Pedersen, T.; Lindh, R.; Reiher, M.; Gonzalez, L. *Phys. Chem. Chem. Phys.* **2015**, *17*, 14383−14392.
(37) Also known as *trans*-$[RuCl(py)_4(NO)]^{2+}$ and *trans*-$[Ru(py)_4Cl(NO)]^{2+}$.
(38) De Candia, A. G.; Marcolongo, J. P.; Etchenique, R.; Slep, L. D. *Inorg. Chem.* **2010**, *49*, 6925−6930.
(39) Merkle, A. C.; Fry, N. L.; Mascharak, P. K.; Lehnert, N. *Inorg. Chem.* **2011**, *50*, 12192−12203.
(40) Fry, N. L.; Mascharak, P. K. *Dalton Trans.* **2012**, *41*, 4726.
(41) Ciofini, I.; Daul, C. A.; Adamo, C. *J. Phys. Chem. A* **2003**, *107*, 11182−11190.
(42) Ciofini, I.; Lainé, P. P.; Bedioui, F.; Daul, C. A.; Adamo, C. *C. R. Chim.* **2006**, *9*, 226−239.
(43) Göttle, A. J.; Dixon, I. M.; Alary, F.; Heully, J.-L.; Boggio-Pasqua, M. *J. Am. Chem. Soc.* **2011**, *133*, 9172−9174.
(44) Vieuxmaire, O. P. J.; Piau, R. E.; Alary, F.; Heully, J.-L.; Sutra, P.; Igau, A.; Boggio-Pasqua, M. *J. Phys. Chem. A* **2013**, *117*, 12821−12830.
(45) Göttle, A. J.; Alary, F.; Dixon, I. M.; Heully, J.-L.; Boggio-Pasqua, M. *Inorg. Chem.* **2014**, *53*, 6752−6760.
(46) Atanasov, M.; Schönherr, T. *J. Mol. Struct.: THEOCHEM* **2002**, *592*, 79−93.
(47) Karidi, K.; Garoufis, A.; Tsipis, A.; Hadjiliadis, N.; den Dulk, H.; Reedijk, J. *Dalton Trans.* **2005**, *7*, 1176−1187.
(48) Kurtikyan, T. S.; Hayrapetyan, V. A.; Martirosyan, G. G.; Ghazaryan, R. K.; Iretskii, A. V.; Zhao, H.; Pierloot, K.; Ford, P. C. *Chem. Commun.* **2012**, *48*, 12088−12090.
(49) Freitag, L.; González, L. *Inorg. Chem.* **2014**, *53*, 6415−6426.
(50) Frisch, M. J.; et al. *Gaussian 09*, revision D.01; Gaussian, Inc.: Wallingford, CT, 2010.
(51) Lee, C.; Yang, W.; Parr, R. G. *Phys. Rev. B: Condens. Matter Mater. Phys.* **1988**, *37*, 785.
(52) Becke, A. D. *J. Chem. Phys.* **1993**, *98*, 5648.
(53) Grimme, S.; Antony, J.; Ehrlich, S.; Krieg, H. *J. Chem. Phys.* **2010**, *132*, 154104.
(54) Schäfer, A.; Horn, H.; Ahlrichs, R. *J. Chem. Phys.* **1992**, *97*, 2571.
(55) Andrae, D.; Haeussermann, U.; Dolg, M.; Stoll, H.; Preuss, H. *Theor. Chim. Acta* **1990**, *77*, 123−141.
(56) Martin, J. M. L.; Sundermann, A. *J. Chem. Phys.* **2001**, *114*, 3408.
(57) Neese, F. *WIREs: Comput. Mol. Sci.* **2012**, *2*, 73−78.
(58) Coe, B. J.; Meyer, T. J.; White, P. S. *Inorg. Chem.* **1995**, *34*, 593−602.
(59) Sinnecker, S.; Rajendran, A.; Klamt, A.; Diedenhofen, M.; Neese, F. *J. Phys. Chem. A* **2006**, *110*, 2235−2245.
(60) Tao, J.; Perdew, J. P.; Staroverov, V. N.; Scuseria, G. E. *Phys. Rev. Lett.* **2003**, *91*, 146401.
(61) Hirata, S.; Head-Gordon, M. *Chem. Phys. Lett.* **1999**, *314*, 291−299.
(62) Hirata, S.; Head-Gordon, M. *Chem. Phys. Lett.* **1999**, *302*, 375−382.
(63) Martin, R. L. *J. Chem. Phys.* **2003**, *118*, 4775−4777.
(64) Angeli, C.; Cimiraglia, R.; Evangelisti, S.; Leininger, T.; Malrieu, J.-P. *J. Chem. Phys.* **2001**, *114*, 10252−10264.
(65) Angeli, C.; Cimiraglia, R.; Malrieu, J.-P. *Chem. Phys. Lett.* **2001**, *350*, 297−305.

DOI: 10.1021/acs.inorgchem.5b00998
Inorg. Chem. 2015, 54, 8310−8318

(66) Angeli, C.; Cimiraglia, R.; Malrieu, J.-P. *J. Chem. Phys.* **2002**, *117*, 9138−9153.
(67) Schmidt, M. W.; Baldridge, K. K.; Boatz, J. A.; Elbert, S. T.; Gordon, M. S.; Jensen, J. H.; Koseki, S.; Matsunaga, N.; Nguyen, K. A.; Su, S.; Windus, T. L.; Dupuis, M.; Montgomery, J. A. *J. Comput. Chem.* **1993**, *14*, 1347−1363.
(68) Zahariev, F.; Gordon, M. S. *J. Chem. Phys.* **2014**, *140*, 18A523.
(69) Friese, D. H.; Beerepoot, M. T. P.; Ringholm, M.; Ruud, K. *J. Chem. Theory Comput.* **2015**, *11*, 1129.
(70) Glendening, E. D.; et al. *NBO 6.0*; Theoretical Chemistry Institute, University of Wisconsin, Madison, WI, 2013.
(71) Glendening, E. D.; Landis, C. R.; Weinhold, F. *J. Comput. Chem.* **2013**, *34*, 1429−1437.
(72) In general, the common ^{1}MLCT states in ruthenium(II) polypyridine complexes consist of electronic promotions from a Ru(d) orbital to a pure ligand orbital. In this particular case, the orbital that receives the electron is unusual because it also has a nonnegligible metallic contribution.
(73) King, A. W.; Jin, Y.; Engle, J. T.; Ziegler, C. J.; Rack, J. J. *Inorg. Chem.* **2013**, *52*, 2086−2093.
(74) King, A. W.; McClure, B. A.; Jin, Y.; Rack, J. J. *J. Phys. Chem. A* **2014**, *118*, 10425−10432.
(75) Heully, J.-L.; Alary, F.; Boggio-Pasqua, M. *J. Chem. Phys.* **2009**, *131*, 184308.
(76) Balzani, V.; Ceroni, P.; Juris, A. *Photochemistry and Photophysics: Concepts, Research, Applications*, 1st ed.; Wiley-VCH: Weinheim, Germany, 2014; references cited therein.
(77) Salassa, L.; Garino, C.; Salassa, G.; Gobetto, R.; Nervi, C. *J. Am. Chem. Soc.* **2008**, *130*, 9590−9597.
(78) Ishikawa, T.; Tanaka, K. *Z. Kristallogr.* **2008**, *223*, 334−342.
(79) Adamo, C.; Barone, V. *J. Chem. Phys.* **1999**, *110*, 6158−6170.
(80) Xu, X.; Goddard, W. A. *Proc. Natl. Acad. Sci. U. S. A.* **2004**, *101*, 2673−2677.
(81) Chai, J.-D.; Head-Gordon, M. *J. Chem. Phys.* **2008**, *128*, 084106.
(82) Perdew, J. P.; Burke, K.; Ernzerhof, M. *Phys. Rev. Lett.* **1996**, *77*, 3865−3868.
(83) Perdew, J. P.; Burke, K.; Ernzerhof, M. *Phys. Rev. Lett.* **1997**, *78*, 1396−1396.
(84) Hauser, A.; Enachescu, C.; Daku, M. L.; Vargas, A.; Amstutz, N. *Coord. Chem. Rev.* **2006**, *250*, 1642−1652.

DOI: 10.1021/acs.inorgchem.5b00998
Inorg. Chem. 2015, 54, 8310−8318